First-principles study of magnetic properties in Fe-ladder compound $BaFe_2S_3$

Michi-To Suzuki,[1] Ryotaro Arita,[1] and Hiroaki Ikeda[2]
[1]*RIKEN, Center for Emergent Matter Science, 2-12-1 Hirosawa, Wako, Saitama 351-0198, Japan*
[2]*Department of Physical Sciences, Ritsumeikan University, 1-1-1 Nojihigasi, Kusatsu, Shiga 525-8577, Japan*
(Received 10 June 2015; published 10 August 2015)

We study the magnetic, structural, and electronic properties of the recently discovered iron-based superconductor $BaFe_2S_3$ based on density functional theory with the generalized gradient approximation. The calculations show that the magnetic alignment in which the spins are coupled ferromagnetically along the rung and antiferromagnetically along the leg is the most stable in the possible magnetic structure within an Fe ladder and is further stabilized with the periodicity characterized by the wave vector $\mathbf{Q}=(\pi,\pi,0)$, leading to the experimentally observed magnetic ground state. The magnetic exchange interaction between the Fe ladders creates a tiny energy gap, the size of which is in excellent agreement with the experiments. Applied pressure suppresses the energy gap and leads to an insulator-metal transition. Finally, we also discuss what type of orbitals can play crucial roles on the magnetic and insulator-metal transition.

DOI: 10.1103/PhysRevB.92.085116 PACS number(s): 71.27.+a, 71.20.Be, 75.10.Lp, 74.20.Pq

I. INTRODUCTION

The discovery of superconductivity in fluorine doped LaFeAsO has stimulated intensive studies of iron-based superconductors [1]. In addition to the high superconducting transition temperature and the strong flexibility for the constituent atoms, similarities of magnetic and structural properties with the high-T_c cuprate superconductors are suggestive to understand the pairing mechanism [2]. For instance, the parent material undergoes antiferromagnetic transition under ambient pressure, and the superconducting transition appears in the vicinity of the antiferromagnetic phase by doping carriers or by applying pressure.

Recently, superconductivity in $BaFe_2S_3$ has been discovered under pressure with the maximum $T_c \sim 14$ K [3]. Investigation of the magnetic and electronic properties in relation to the structural property in this ladder system is expected to provide a new path to understand the high-T_c superconductivity in the iron-based superconductors. The quasi-one-dimensional Fe-ladder formation of $BaFe_2S_3$, as shown in Fig. 1, exhibits a striking difference from the conventional iron-based superconductors, which have two-dimensional Fe networks, but rather reminds us of the superconducting two-leg ladder cuprate $Sr_{14}Cu_{24}O_{41}$ [4]. While the magnetic structure of $BaFe_2S_3$ has a marked similarity to conventional iron-based superconductors as will be discussed below, $BaFe_2S_3$ has a semiconducting ground state as contrasted to the metallic ground states of other iron-based superconductors.

A number of structurally related compounds of $BaFe_2S_3$, i.e., AFe_2X_3 (A = K, Rb, Cs, or Ba and X = S, Se, or Te), have been discovered [5–7]. In particular, the block magnetism of $BaFe_2Se_3$ has attracted increasing attention as the novel magnetic structure among iron-based materials and has been intensively studied both theoretically [8–13] and experimentally [5,14–22]. On the other hand, the physical properties of $BaFe_2S_3$ are reported only recently in association with the discovery of the high-T_c superconducting transition [3]. $BaFe_2S_3$ crystallizes in an orthorhombic crystal structure, the symmetry of which belongs to space group $Cmcm$ (no. 63), which is the same as those of $CsFe_2Se_3$ and KFe_2Se_3 [18,23] but is different from $Pnma$ (no. 62) of $BaFe_2Se_3$ [5]. The crystal structure of $BaFe_2S_3$ is shown in Fig. 1. We see that Fe atoms form two-leg ladders running along the c axis. All Ba atoms and some S atoms are on the planes including the y axis and the lines across the middle of the rungs, and the other S atoms are located in the space between the nearest Fe ladders.

While the block magnetism in $BaFe_2Se_3$ is characterized by $\mathbf{Q}=(\pi,\pi,\pi)$, the periodicity of the stripe magnetism in $BaFe_2S_3$ is characterized by $\mathbf{Q}=(\pi,\pi,0)$. The same stripe-type magnetism with $BaFe_2S_3$ is also observed in $CsFe_2Se_3$ and KFe_2Se_3. The local magnetic moment of iron is reported as $1.2\mu_B$ in $BaFe_2S_3$ [3], which is quite smaller than $1.8\mu_B$ of $CsFe_2Se_3$ [23] and $2.8\mu_B$ of $BaFe_2Se_3$ [17], and the Néel temperatures of 120, 175, and 255 K for $BaFe_2S_3$, $CsFe_2Se_3$, and $BaFe_2Se_3$, respectively, are corresponding to the size of the magnetic moments. The activation energy of $BaFe_2S_3$ is reported to be less than 0.1 eV [24,25], which is again smaller than 0.13 and 0.178 eV reported for $BaFe_2Se_3$ [17,22] and 0.34 eV for $CsFe_2Se_3$ [23].

The first-principles study for iron-based superconductors has provided fruitful information concerning the structural, magnetic, and electronic properties [26–32]. For $BaFe_2S_3$, we recently derived a low-energy effective Hamiltonian based on a first-principles approach [33]. In this paper, we investigate the magnetic and electronic properties in relation to the structural property under pressure by using the first-principles calculations based on the generalized gradient approximation (GGA). We show that the stripe spin-ladder magnetic order, which is shown in type-I magnetic configuration in Fig. 2 with the ordering wave vector $\mathbf{Q}=(\pi,\pi,0)$, is the most stable magnetic structure over the investigated range of pressure. We also discuss how the electronic structure changes under pressure and undergoes a metal-insulator transition, which is necessary for the superconducting transition.

II. METHOD

The first-principles calculations are implemented in the VASP program code with the projector augmented-wave method using the exchange-correlation functional proposed by Perdew, Burke, and Ernzerhof [34]. We systematically explored all the possible spin configurations within the Fe

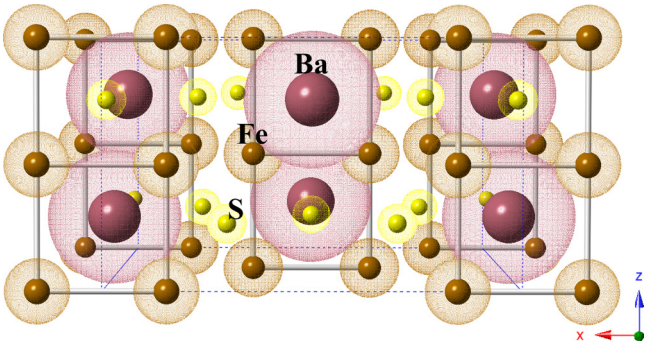

FIG. 1. (Color online) Crystal structure of $BaFe_2S_3$.

ladder, as shown in Fig. 2, for the characteristic wave vectors **Q**=(0,0,0), (π,0,0), (π,π,0), setting the 2×2×1 supercell, corresponding to the magnetic unit cell for the periodicity characterized by **Q**=(π,π,0). The k-point mesh is set as (2,2,2) for the self-consistent calculations and (8,8,8) for plotting the density of states (DOS) for the calculations of the supercell. The calculations were performed with the experimental lattice constants a = 8.78 Å, b = 11.23 Å, c = 5.29 Å for ambient pressure, and the pressure effect is considered as change in the lattice constants observed experimentally under hydrostatic pressure [35]. The atomic relaxation is performed for the sulfur atoms within the x-y plane, starting from the initial atomic configuration as the experimental values under ambient pressure, i.e., Ba(4c) (0.0,0.686,0.25), Fe(8e) (0.154,0.0,0.0),

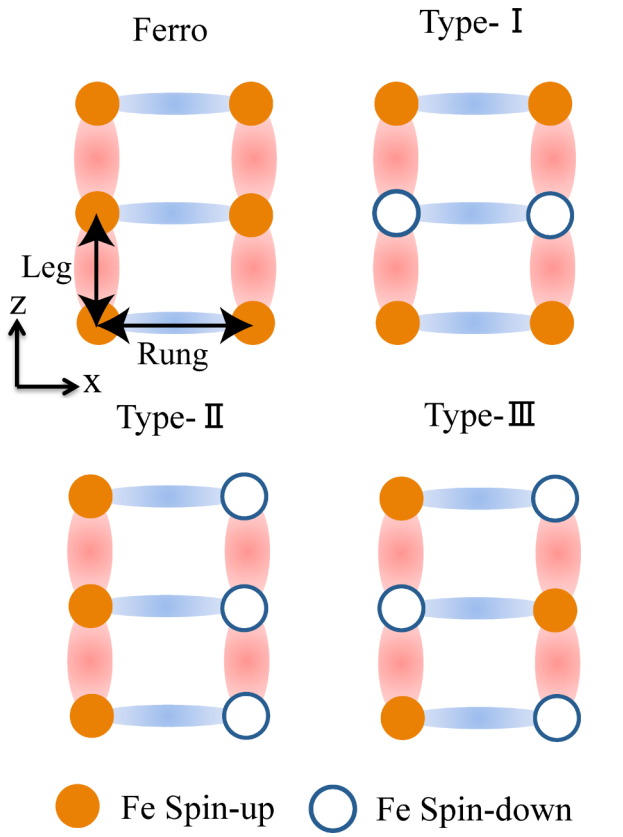

FIG. 2. (Color online) Possible inequivalent magnetic configurations within the Fe ladder.

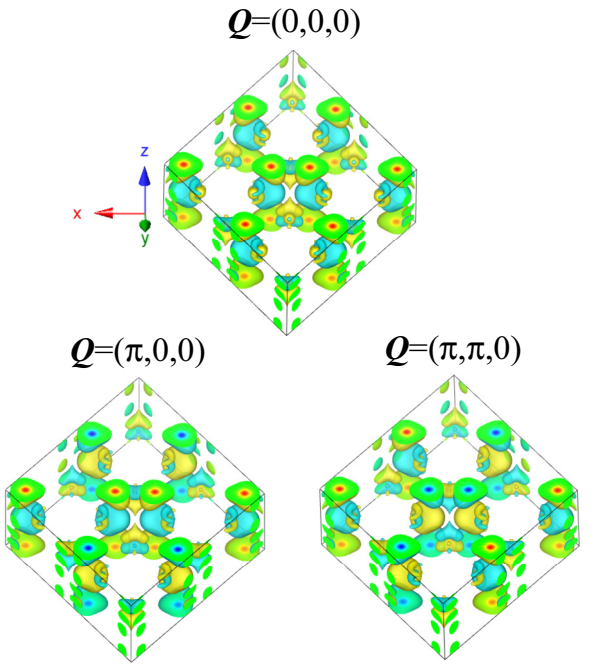

FIG. 3. (Color online) Computed spin distribution of the type-I magnetic order characterized by **Q**=(0,0,0), (π,0,0), (π,π,0). The yellow (blue) surface is an isosurface of positive (negative) spin density.

S(4c) (0.0, 0.116, 0.25), and S(8g) (0.208, 0.378, 0.25), using the experimental lattice constants [35]. The energy cutoff for the plane waves is set as 500 eV through the calculations. The convergence conditions for the total energies are set as 10^{-5} eV for the electronic self-consistent loop and 10^{-2} eV for the ionic relaxation.

III. RESULTS

First, we discuss the stable magnetic structure of $BaFe_2S_3$. The magnetic distributions of type-I magnetism with different **Q** are shown in Fig. 3. Calculated total energies and Fe magnetic moments are shown in Table I. As shown in the table, the calculations predict the most stable magnetic structure as the type-I magnetic alignment, in which the spins are coupled ferromagnetically along the rung and antiferromagnetically along the leg, with the periodicity characterized by **Q**=(π,π,0), which corresponds to the experimentally observed magnetic alignment. The energy difference is mainly dominated by the spin configuration within the Fe ladders, changing the total energy with the order of 1 eV, and the different **Q** structure changes it with the order of 0.1 eV.

Relaxation of sulfur atoms somewhat reduces the magnetic moments from those for the experimental atomic position for the type-I, -II, and -III magnetic states and completely suppresses it for FM spin alignment. Remarkably, the type-I magnetic configuration is the most stable magnetic structure within an Fe ladder in spite of the smaller magnetic moments compared to those of type II. This result indicates that the atomic configuration strongly affects stabilization of the type-I magnetism through coupling with the magnetic moments. The predicted Fe magnetic moment 2.07μ_B of the type-I magnetic

TABLE I. Total energies and spin moments calculated for the different spin configurations (see text).

	Experimental structure ($P = 0$)		Optimized structure ($P = 0$)		Optimized structure (P=16.27 GPa)	
	Total energy (eV)	Fe moment (μ_B)	Total energy (eV)	Fe moment (μ_B)	Total energy (eV)	Fe moment (μ_B)
			Ferro			
Q=(0,0,0)	−291.006	1.28	−293.901	0.00	−293.296	0.00
Q=(π,0,0)	−290.786	1.08	−293.901	0.00	−293.295	0.00
Q=(π,π,0)	−291.050	1.03	−293.901	0.00	−293.296	0.00
			Type I			
Q=(0,0,0)	−296.009	2.26	−296.778	2.08	−293.558	1.42
Q=(π,0,0)	−295.967	2.27	−296.742	2.08	−293.632	1.10
Q=(π,π,0)	−296.045	2.27	−296.809	2.07	−293.672	1.40
			Type II			
Q=(0,0,0)	−294.964	2.55	−295.245	2.42	−293.296	0.00
Q=(π,0,0)	−294.953	2.49	−295.310	2.31	−293.296	0.00
Q=(π,π,0)	−294.653	2.49	−295.043	2.30	−293.296	0.00
			Type III			
Q=(0,0,0)	−294.402	2.15	−295.314	1.87	−293.295	0.15
Q=(π,0,0)	−294.259	2.14	−295.182	1.89	−293.296	0.00
Q=(π,π,0)	−294.281	2.15	−295.195	1.86	−293.295	0.14

order is considerably larger than the experimental value 1.3μ_B, and this kind of overestimation for Fe moments was also reported for LaFeAsO [26–30,36,37].

We also investigated the magnetic states under pressure by using the experimental lattice constants with performing relaxation of sulfur atoms. As shown in Table I, whereas the magnetic moments of the type-I magnetic states are not much reduced at P=16.27 GPa, those of the other magnetic states are strongly suppressed under high pressure. To examine the pressure dependence of the magnetic states in further detail, we show in Fig. 4 the detailed pressure dependence of the total energies and Fe-spin moments for the magnetic states with the periodicity **Q**=(π,π,0). From the figure we can find a clear difference in the pressure dependence for all of the magnetic structures, though the type-I, -II, and -III magnetisms exhibit the same order of the magnetic moments at ambient pressure. The pressure effect strongly suppresses the magnetic moments of the type-II magnetism, in which the magnetic moment vanishes already at P=2 GPa and gradually suppress the magnetic moments of the type-III magnetism, leading to the nonmagnetic state around 16 GPa. On the other hand, the pressure dependence of the magnetic moment for the type-I magnetism is rather weak and leaves the magnetic order stable even under high pressure.

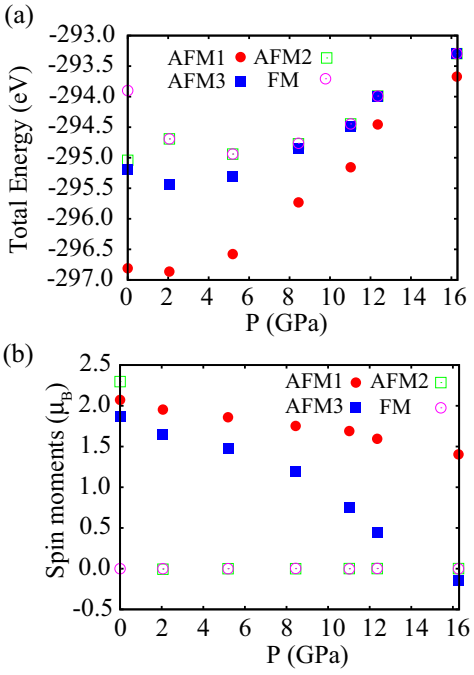

FIG. 4. (Color online) Pressure dependence of (a) total energy and (b) magnetic moments for all possible magnetic structures characterized by **Q** =(π,π,0).

The optimized sulfur positions, the coordinates of which are defined in Fig. 5, are y_{S1}=1.18 Å, x_{S2}=$x_{S2'}$=2.52 Å, and y_{S2}= $y_{S2'}$=1.36 Å while the experimental positions are y_{S1}=1.30 Å, x_{S2}=$x_{S2'}$=2.57 Å, and y_{S2}=$y_{S2'}$=1.37 Å. The deviation between the calculation and the experiment for the S1 position is somewhat larger than that for the S2 atom, yet the deviations are about 1% at most for the lattice constants. We also show the pressure dependence of the sulfur's atomic positions in Fig. 5, in which the positions of sulfurs are measured from the Fe ladder as defined in Fig. 5(a). Interestingly, from Fig. 5(b), significant shifts in the sulfur positions are only observed for the sulfurs out of the Fe ladders (S2 and S2'), and the positions of sulfurs located between the ladder's legs (S1) do not strongly depend on the pressure. Note that S2 and S2' in Fig. 5 are equivalent in the nonmagnetic crystal structure but are inequivalent in the magnetic state. The calculations indeed show small deviation of the two sulfur positions above $P \sim$ 12 GPa as shown in Fig. 5(b).

Finally, we discuss the electronic structure of $BaFe_2S_3$. Experimentally, $BaFe_2S_3$ is a semiconductor with a small energy gap of 0.06–0.07 eV [24,25]. As shown in Fig. 6, the energy gap of the $BaFe_2S_3$ is not produced with the **Q**=(0,0,0) periodicity but produced with the periodicity of **Q**=(π,π,0) with the size 0.07 eV for type-I magnetism, which is in

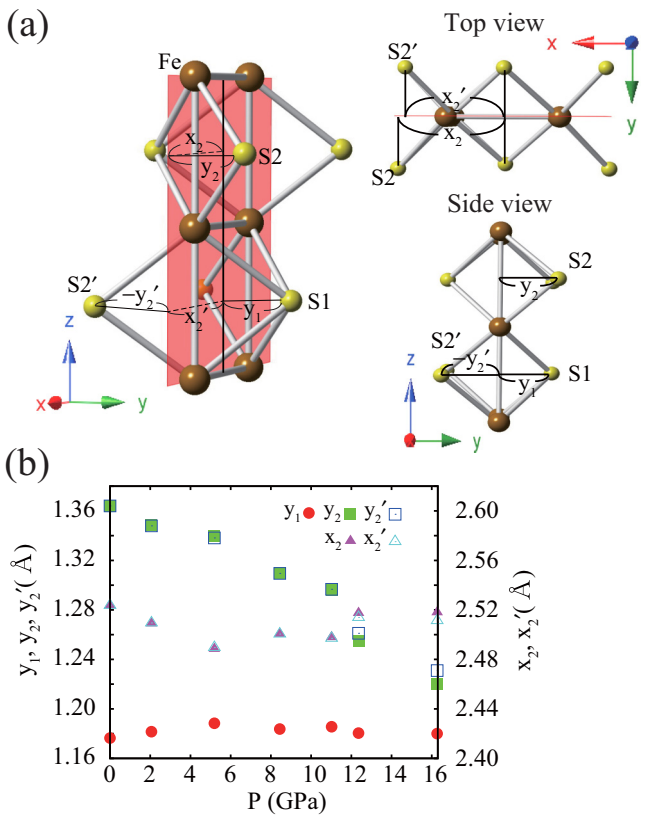

FIG. 5. (Color online) (a) Definitions of sulfur's relative positions and (b) the calculated values for the type-I magnetic states. The red surface sheet in figure (a) indicates a surface on which the Fe ladder lies.

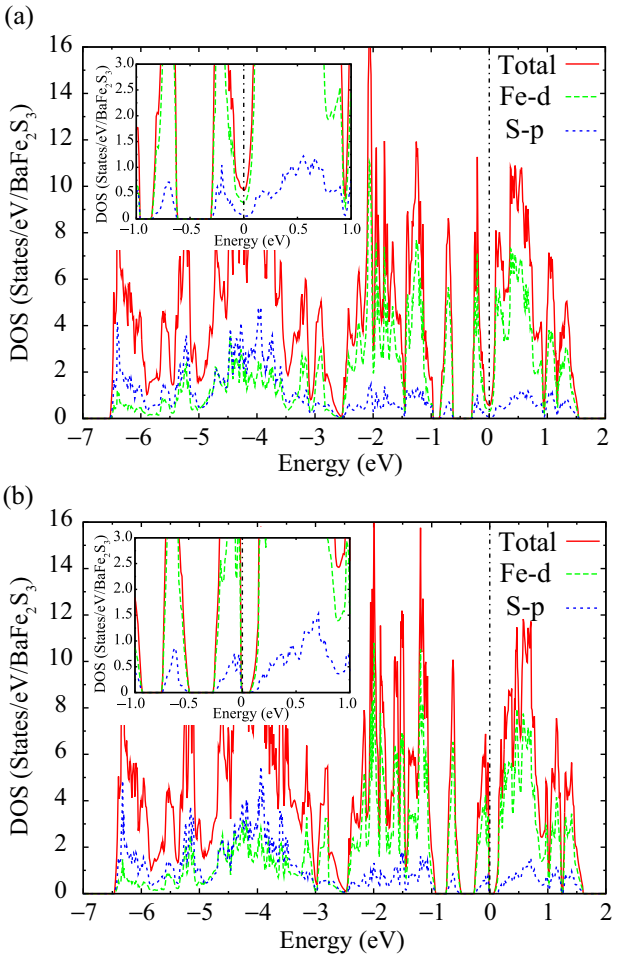

FIG. 6. (Color online) Density of states of type-I AFM magnetic ordered states with the periodicity characterized by **Q**=(0,0,0) and (π,π,0). Insets are the enlarged views around the Fermi levels.

excellent agreement with the experimental evaluations. This result indicates that the magnetic exchange coupling between the Fe ladders is crucial to create the tiny energy gap. Figure 7 shows pressure dependence of total DOS for the **Q**=(π,π,0) type-I antiferromagnetic states around the Fermi level. The pressure strongly suppresses the energy gap and leads to a metallic state around $P \sim 5$ GPa. The peak structure of DOS located below the Fermi level comes close to the Fermi level as the pressure increases and passes over the Fermi level at $P \sim 12$ GPa. As a result, pressure strongly enhances the DOS at the Fermi level which takes its maximum at $P \sim 12$ GPa. The orbital resolved DOS of Fe-d orbitals for the pressure P=0 and 12.36 GPa is shown in Fig. 8. The large difference in the structure of the DOS for the majority and minority spin indicates that all of the Fe-d orbitals contribute to the magnetic order. More precisely, contribution for the spin moment of each d orbital calculated from the spin DOS is 0.37 (0.28) for d_{xy}, 0.39 (0.30) for d_{yz}, 0.34 (0.27) for $d_{3z^2-r^2}$, 0.47 (0.36) for d_{xz}, and 0.49 (0.37) for $d_{x^2-y^2}$, leading to the total Fe-d moment 2.06 (1.58), at P=0 (12.36 GPa). The larger magnetic moments of the d_{xz} and $d_{x^2-y^2}$ orbitals compared to other d orbitals show the primary contribution of these two orbitals for the magnetism, which is consistent with our recent studies showing that low-energy effective Hamiltonians can be constructed from these two orbitals [33]. The $d_{3z^2-r^2}$ orbital mainly contributes to the DOS peak below the Fermi level at ambient pressure but applied pressure suppresses it as in Figs. 8(b) and 8(d). Alternatively, the d_{yz} and the $d_{x^2-y^2}$ orbitals develop with applied pressure and contribute to the maximum DOS peak at Fermi level at $P \sim 12$ GPa. Although further investigation is necessary to reveal the orbital contribution to the superconducting transition, the interplay of

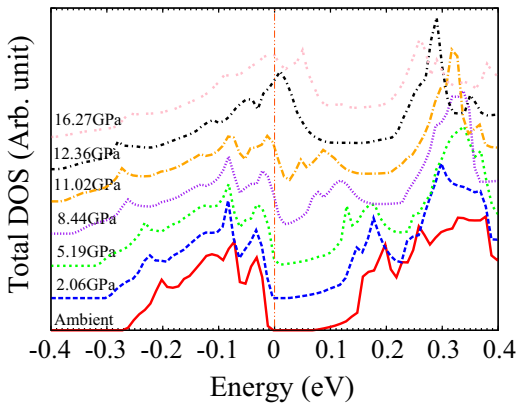

FIG. 7. (Color online) Pressure dependence of density of states for type-I AFM magnetic ordered states with the periodicity of Q = (π,π,**0**).

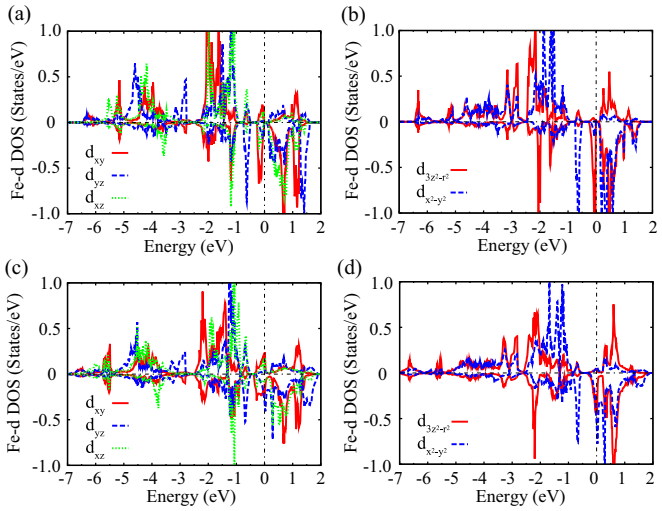

FIG. 8. (Color online) Density of states of Fe-d orbitals for type-I [$\mathbf{Q}$=(π,π,0)] AFM states for P=0 and 12.36 GPa.

these Fe-d orbitals should be crucial for the high-T_c transition temperature.

IV. CONCLUSION

We investigated the magnetic, structural, and electronic properties of $BaFe_2S_3$ based on first-principles calculations. The GGA calculations predicted stripe-type spin-ladder magnetism, the magnetic periodicity of which is characterized by $\mathbf{Q}$=(π,π,0), in the ground state. The calculations of the pressure dependence for the total energy and magnetic moments indicate that the most stable type-I magnetic structure is not sensitive against the applied pressure compared to other magnetic structures and leaves the magnetic order stable even at high pressure as a result. The magnetic exchange interaction between the Fe ladders creates a tiny energy gap at ambient pressure and is therefore a crucial ingredient to reproduce the insulating magnetic ground state as observed experimentally. Applied pressure strongly suppresses the energy gap and leads to a metallic magnetic state, bringing a high DOS at the Fermi level due to the formation of DOS peak structure around the Fermi level. The magnetic moment predicted at ambient pressure is considerably larger than that observed experimentally. The discrepancy of the magnetic states may be improved with a more advanced first-principles method considering the strong electron correlation in the iron-based compound [36–41], and more precise prediction of the magnetic states is our future issue.

ACKNOWLEDGMENTS

We thank K. Ohgushi, H. Takahashi, J. Yamaura, and Y. Nambu for providing us their experimental information prior to its publication [3]. This work was supported by Japan Society for the Promotion of Science KAKENHI (Grants No. 15K17713, M.T.S.; Nos. 15H02014 and 15H05745, H.I.; and No. 15H03696, R.A.).

[1] Y. Kamihara, T. Watanabe, M. Hirano, and H. Hosono, J. Am. Chem. Soc. **130**, 3296 (2008).
[2] D. J. Scalapino, Rev. Mod. Phys. **84**, 1383 (2012).
[3] H. Takahashi, A. Sugimoto, Y. Nambu, T. Yamauchi, Y. Hirata, T. Kawakami, M. Avdeev, K. Matsubayashi, F. Du, C. Kawashima, *et al.*, Nat. Mater., doi: 10.1038/nmat4351.
[4] M. Uehara, T. Nagata, J. Akimitsu, and H. Takahashi, N. Môri, and K. Kinoshita, J. Phys. Soc. Jpn. **65**, 2764 (1996).
[5] H. Hong and H. Steinfink, J. Solid State Chem. **5**, 93 (1972).
[6] K. Klepp, W. Sparlinek, and H. Boller, J. Alloys. Compd. **238**, 1 (1996).
[7] M. Reissner, W. Steiner, J. Wernisch, and H. Boller, Hyperfine Interact. **169**, 1301 (2006).
[8] W. Li, C. Setty, X. Chen, and J. Hu, Front. Phys. **9**, 465 (2014).
[9] Q. Luo, K. Foyevtsova, G. D. Samolyuk, F. Reboredo, and E. Dagotto, Phys. Rev. B **90**, 035128 (2014).
[10] E. Dagotto, Rev. Mod. Phys **85**, 849 (2013).
[11] Q. Luo, A. Nicholson, J. Rincón, S. Liang, J. Riera, G. Alvarez, L. Wang, W. Ku, G. D. Samolyuk, A. Moreo *et al.*, Phys. Rev. B **87**, 024404 (2013).
[12] W. Lv, A. Moreo, and E. Dagotto, Phys. Rev. B **88**, 094508 (2013).
[13] M. V. Medvedev, I. A. Nekrasov, and M. V. Sadovskii, JETP Lett. **95**, 33 (2012).
[14] K. Komedera, A. K. Jasek, A. Blachowski, K. Ruebenbauer, M. Piskorz, J. Zukrowski, A. Krzton-Maziopa, E. Pomjakushina, and K. Conder, Solid State Commun. **207**, 5 (2015).
[15] M. Mourigal, S. Wu, M. B. Stone, J. R. Neilson, J. M. Caron, T. M. McQueen, and C. L. Broholm, Phys. Rev. Lett. **115**, 047401 (2015).
[16] S. W. Lovesey and D. D. Khalyavin, arXiv:1412.2536.
[17] Y. Nambu, K. Ohgushi, S. Suzuki, F. Du, M. Avdeev, Y. Uwatoko, K. Munakata, H. Fukazawa, S. Chi, Y. Ueda *et al.*, Phys. Rev. B **85**, 064413 (2012).
[18] J. M. Caron, J. R. Neilson, D. C. Miller, K. Arpino, and A. Llobet, and T. M. McQueen, Phys. Rev. B **85**, 180405 (2012).
[19] A. Krzton-Maziopa, E. Pomjakushina, V. Pomjakushin, D. Sheptyakov, D. Chernyshov, V. Svitlyk, and K. Conder, J. Phys.: Condens. Matter **23**, 402201 (2011).
[20] J. M. Caron, J. R. Neilson, D. C. Miller, A. Llobet, and T. M. McQueen, Phys. Rev. B **84**, 180409 (2011).
[21] B. Saparov, S. Calder, B. Sipos, H. Cao, S. Chi, D. J. Singh, A. D. Christianson, M. D. Lumsden, and A. S. Sefat, Phys. Rev. B **84**, 245132 (2011).
[22] H. Lei, H. Ryu, A. I. Frenkel, and C. Petrovic, Phys. Rev. B **84**, 214511 (2011).
[23] F. Du, K. Ohgushi, Y. Nambu, T. Kawakami, M. Avdeev, Y. Hirata, Y. Watanabe, T. J. Sato, and Y. Ueda, Phys. Rev. B **85**, 214436 (2012).
[24] Z. S. Gönen, P. Fournier, V. Smolyaninova, R. Greene, F. M. Araujo-Moreira, and B. Eichhorn, Chem. Mater. **12**, 3331 (2000).
[25] W. Reiff, I. Grey, A. Fan, Z. Eliezer, and H. Steinfink, J. Solid State Chem. **13**, 32 (1975).

[26] S. Ishibashi, K. Terakura, and H. Hosono, J. Phys. Soc. Jpn. **77**, 053709 (2008).
[27] S. Ishibashi and K. Terakura, J. Phys. Soc. Jpn. **77**, 91 (2008).
[28] I. I. Mazin, M. D. Johannes, L. Boeri, K. Koepernik, and D. J. Singh, Phys. Rev. B **78**, 085104 (2008).
[29] I. I. Mazin and M. D. Johannes, Nat. Phys. **5**, 141 (2008).
[30] Z. P. Yin, S. Lebegue, M. J. Han, B. P. Neal, S. Y. Savrasov, and W. E. Pickett, Phys. Rev. Lett. **101**, 047001 (2008).
[31] T. Yildirim, Phys. Rev. Lett. **101**, 057010 (2008).
[32] T. Yildirim, Physica C **469**, 425 (2009).
[33] R. Arita, H. Ikeda, S. Sakai, and M.-T. Suzuki (unpublished).
[34] J. P. Perdew, K. Burke, M. Ernzerhof, Phys. Rev. Lett. **77**, 3865 (1996).
[35] Y. Hirata, S. Maki, J.-i. Yamaura, T. Yamauchi, and K. Ohgushi, arXiv:1507.06047.
[36] P. Hansmann, R. Arita, A. Toschi, S. Sakai, and G. Sangiovanni, and K. Held, Phys. Rev. Lett. **104**, 197002 (2010).
[37] A. Toschi, R. Arita, P. Hansmann, G. Sangiovanni, and K. Held, Phys. Rev. B **86**, 064411 (2012).
[38] Q. Si and E. Abrahams, Phys. Rev. Lett. **101**, 076401 (2008).
[39] Z. Yin, K. Haule, and G. Kotliar, Nat. Phys. **7**, 294 (2011).
[40] Z. Yin, K. Haule, and G. Kotliar, Nat. Mater. **10**, 932 (2011).
[41] T. Schickling, F. Gebhard, J. Bünemann, L. Boeri, O. K. Andersen, and W. Weber, Phys. Rev. Lett. **108**, 036406 (2012).